# Defect dynamics in crystalline buckled membranes

Aldo D. Pezzutti and Daniel A. Vega*

*Department of Physics and Instituto de Física del Sur, Universidad Nacional del Sur–CONICET, Av L.N. Além 1253. (8000), Bahía Blanca, Argentina*

(Received 6 March 2011; revised manuscript received 30 May 2011; published 18 July 2011)

We study the dynamics of defect annihilation in flexible crystalline membranes suffering a symmetry-breaking phase transition. The kinetic process leading the system toward equilibrium is described through a Brazovskii-Helfrich-Canham Hamiltonian. In membranes, a negative disclination has a larger energy than a positive disclination. Here we show that this energetic asymmetry does not only affect equilibrium properties, like the Kosterlitz-Thouless transition temperature, but also plays a fundamental role in the dynamic of defects. Both unbinding of dislocations and Carraro-Nelson "antiferromagnetic" interactions between disclinations slow down the dynamics below the Lifshitz-Safran regime observed in flat hexagonal systems.

DOI: 10.1103/PhysRevE.84.011123 PACS number(s): 64.60.−i, 61.72.Bb, 61.46.−w, 81.07.−b

## I. INTRODUCTION

Spatially periodic patterns are ubiquitous in nature because ordered configurations frequently minimize the interaction potential between the building blocks of a wide variety of systems [1]. Besides the academic interest, the studies of pattern formation in low-dimensional systems also have been driven by the potential applications to soft matter, biophysics, and nanotechnology. For example, thin-film patterns of block copolymers have been used as nanolithographic masks for pattern transfer [2,3] and the synthesis of graphene, a two-dimensional material with unprecedented physical properties, has opened new horizons for science and technology [4]. One of the main difficulties associated with these systems for practical applications is the lack of long-range order due to the presence of topological defects that often control key material properties [5–8]. For example, the nonlocal disorder introduced by disclinations in smectic systems reduces the applicability to several nanodevices [8,9], and the fact that graphene is actually not flat but exhibits pronounced wrinkles into the third dimension was attributed to the presence of defects, like dislocations and grain boundaries [4]. However, defects are not necessarily undesirable. For example, it has been suggested that novel tetravalent colloidal materials can be developed by anchoring chemical linkers or DNA strands to the topological defects of nematic textures lying on the surface of micron-sized spheres [10,11]. And more recently, it has been shown that grain boundaries can be used as tunable transport gaps to develop practical digital electronic devices based on graphene [12]. However, although in some cases the diffusion of defects and grain boundaries can be arrested by an appropriate selection of the material properties, defect motion is a thermally activated process that can disturb both crystalline order and transport properties.

During the last years there has been an increasing interest in the study of two-dimensional (2D) textures on curved surfaces [13–19]. One of the main differences between planar and curved 2D-modulated phases is related to the structure of topological defects. While in most flat systems the defects are nontrivial excitations of the ground state, in the case of curved crystals long-range interactions can lead to complex arrays of defects even at zero temperature [18].

Although the equilibrium properties of crystalline membranes have been well established [20–24], how the dynamics of defects is affected by the curvature of the space in which the system lives is an open question that we address in this paper. This study is focused in a membrane with internal degrees of freedom, that below a critical temperature undergoes a symmetry-breaking phase transition.

## II. THE MODEL

To describe the dynamic of defects in a crystalline membrane we propose a minimal model that includes a Brazovskii Hamiltonian geometrically coupled to the topography of the membrane. We consider a membrane that at high temperatures is a disordered structureless deformable surface, with equilibrium properties dictated by a Helfrich-Canham Hamiltonian. The low-temperature phase is described through the Brazovskii model, where the fluid membrane phase separates into a buckled crystalline state with hexagonal symmetry.

### A. Fluid membrane

Fluid membranes occur in a wide variety of systems, including surfactant films, vesicles, and lipid bilayer membranes [25–27]. The phase behavior and equilibrium structure of fluid membranes have been investigated intensively in recent years through different methods, including Monte Carlo [28,29], molecular dynamics [30], and phase field models [27].

Here we employ a phase-field approach to describe the temporal evolution of the morphology of the membrane during a symmetry-breaking phase transition. This model accounts for bending stiffness, spontaneous curvature, and surface energy. In the Monge gauge, the deformation of a membrane can be described by $\mathbf{r}(x,y) = [\mathbf{x}, h(x,y)]$, where $\mathbf{x} = \{x,y\}$ represents a set of standard Cartesian coordinates in the plane and $z = h(x,y)$ is the out-of-plane deformation of the membrane over the reference plane $\mathbf{x}$ (see Fig. 1). The equilibrium properties of fluid membranes can be described by a Helfrich-Canham Hamiltonian $F_{\mathrm{HC}}$ [23,24,31–36]:

$$F_{\mathrm{HC}} = \int [F_1 + F_2 + F_3]\sqrt{g}dxdy, \qquad (1)$$

*dvega@uns.edu.ar

 

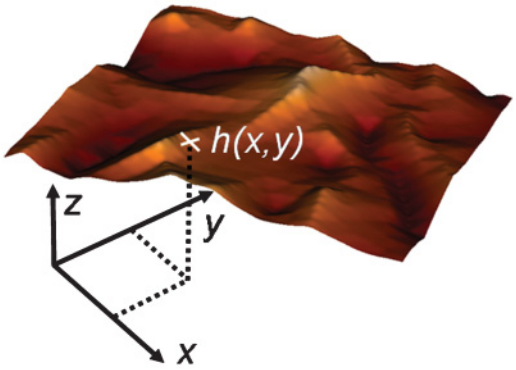


FIG. 1. (Color online) A schematic representation of a crystalline membrane in the Monge gauge. The Monge gauge describes a surface by a single function $z = h(x,y)$, the height over a reference plane $(x,y)$.

where $g$ is the metric tensor [14,23]. The first energy density term $F_1 = \frac{k_B}{2}(K - C_0)^2$ accounts for the bending elastic energy [33,34]. Here $k_B$ is the bending modulus, $K$ is the mean curvature, and $C_0$ the homogeneous spontaneous curvature [33]. The second term $F_2 = \sigma$ is an isotropic contribution that controls the area of the membrane and it is characterized by a constant surface tension $\sigma$. The third energy density contribution $F_3 = \frac{k_g}{2}R$, where $R$ is the Gaussian curvature and $k_g$ is the Gaussian rigidity, is a topological invariant depending only on the genus of the surface [37].

### B. Crystalline phase

In this work the dynamics of topological defects is studied through a continuous phase field model. The dynamics of defects and the process of phase separation have been studied numerically using different approaches such as Monte Carlo or molecular dynamic methods. However, the atomistic simulations are computationally limited in the time and length scales they are able to achieve. The phase field approach employed here naturally incorporates the elasticity of the hexagonal phase and also provides an efficient approach over diffusive time scales. This approach is by now widely used in order to describe different phenomena on atomic and mesoscopic length scales. For example, it has been applied to describe defect dynamics [38–40], pattern formation [1,41], grain boundary melting [42], symmetry-breaking phase transitions [43–45], block copolymers [46], Langmuir films [47], and liquid crystals [48].

In the neighborhood of the critical temperature, the order-disorder transition can be phenomenologically described by a Brazovskii Hamiltonian [43,49] modified to account for the membrane geometry:

$$F_\psi = \int \left(2\left(\nabla^2_{\mathrm{LB}}\psi\right)^2 - 2\nabla_i\psi\nabla^i\psi + \frac{\tau}{2}\psi^2 + \frac{1}{4}\psi^4\right) dA. \tag{2}$$

This free-energy functional is a modified Ginzburg-Landau expansion in the order parameter $\psi(\mathbf{r}) = \phi(\mathbf{r}) - \phi_0$, where $\phi(\mathbf{r})$ is the local composition and $\phi_0$ is the average composition at the critical temperature $T_c$. In the above equation, $\tau = (T_c - T)/T_c$ is the reduced temperature and $\nabla^2_{\mathrm{LB}}$ is the Laplace-Beltrami operator [50,51]. We use the standard index summation convention while subindices and superindices indicate contravariant and covariant vectors, respectively. At low temperatures, $F_\psi$ favors periodic profiles of well-defined wavelength and symmetry [1,38,52]. In off-critical conditions ($\phi_0 \neq 0$), the hexagonal modulations with a dominant wave vector $k_0 = 1/\sqrt{2}$ are preferred due to the the competition between the gradient square term and the term involving the Laplace-Beltrami operator.

### C. Crystalline membrane dynamics

Taking into account both contributions to the free energy, the Hamiltonian for the crystalline membrane results: $F = F_{\mathrm{HC}} + F_\psi$. A dissipative model [36] where the membrane shape and order parameter are coupled through the metric of the membrane can be used to obtain the time evolution of both scalar fields:

$$\frac{\partial\psi}{\partial t} = -\nabla^2_{\mathrm{LB}}\left(\frac{\delta F}{\delta\psi}\right) + \eta_\psi(\mathbf{r},t), \tag{3}$$

$$\frac{\partial h}{\partial t} = -\frac{\delta F}{\delta h} + \eta_h(\mathbf{r},t). \tag{4}$$

Here $\eta_\psi(\mathbf{r},t)$ and $\eta_h(\mathbf{r},t)$ are the random Gaussian noise fields satisfying fluctuation dissipation [53]. The coupled dynamical equations were numerically solved using a semi-implicit pseudospectral algorithm with periodic boundary conditions. The size of the time step $t_0$ ($t_0 = 10^{-4}$), and spatial steps were selected to provide numerical stability [33]. The system size is $L \times L$, where $L = 256$. The results discussed here did not display any detectable finite-size effects.

## III. RESULTS AND DISCUSSION

Shortly after the quench into the unstable region of the phase diagram, the process of phase separation is dictated by the high temperature fluctuations where both $\psi$ and $h$ remain decoupled ($\psi \sim 0$). A linear instability analysis of Eq. (3) indicates that during this characteristic incubation time $t_c$ ($t \sim t_c \sim \tau^{-1}$), there is a continuous amplification of $\psi$ until the anharmonic terms of the free-energy functional triggers the inhomogeneous nucleation of precursors for crystallization [44]. This stage is characterized by growing crystalline domains embedded in the unstructured fluid phase (see Fig. 2).

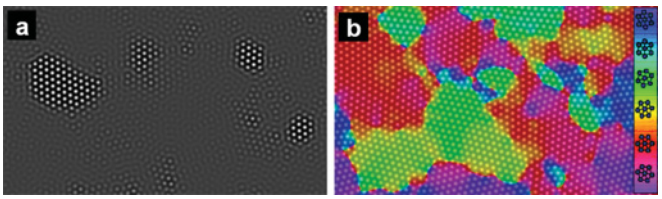


FIG. 2. (Color online) Mechanism of defect formation during the early stage of the phase-separation process. Left panel: nucleation and growth of the orderer phase. The propagating domains with hexagonal symmetry remain roughly flat and free of topological defects. Right panel: the collision of the orientationally uncorrelated domains produces a granular structure with domain walls decorated with dislocations. Here the different colors indicate different grain orientations (color code indicated on the right).

Due to causality, the orientation of distant growing crystals is completely uncorrelated, and the collision of the different domains unavoidably leads to the formation of domain walls decorated with dislocations. Although disclinations also may be present, its strain field is strongly screened by dislocation lines [45,54]. In order to track the temporal evolution of the system, here we identify the defects by means of Voronoi diagrams through the centers of the particles (local maxima of $\psi$) [44,55]. We found that the initial density of topological defects is exclusively determined by the temperature of the quench [45].

It was noted by Park and Lubensky that the crystalline membrane is more rigid than the fluid membrane [23]. Consequently, a crystalline membrane is more crinkled than crumpled and its configuration depends on the distribution of defects. Theoretically, it has been found that the buckling induced by topological defects is determined by the interplay between the strain energy of the defect and the free-energy penalization for curvature [20–23,56]. In hexagonal crystals, disclinations are points of local fivefold or sevenfold symmetry, while dislocations are topological defects formed by disclination dipoles separated by a lattice constant $a_0$ [50,53]. It was found that the buckling occurs when $K_0\ell_0^2/k_B \geqslant \gamma$, where $\ell_0$ is a characteristic length scale and $\gamma$ is a dimensionless constant of order $10^2$. In addition and contrary to flat systems, it has been observed that in the buckled state positive and negative disclinations do not have the same energy. As compared with a positive disclination, a negative disclination has a larger energy and a smaller critical value of $K_0/k_B$ at buckling [24].

In the flat ordered phase the Lamé constants and 2D Young modulus can be determined through the order parameter field [57]. For the hexagonal phase $\psi(r,t) = A_k[\cos(k_0x)\cos(\frac{k_0y}{\sqrt{3}}) - \frac{1}{2}\cos(\frac{2k_0y}{\sqrt{3}})] + \phi_0$, where $A_k = \frac{1}{15}(-3\phi 7_0 + \sqrt{3}\sqrt{20k_0^2 - 20k_0^4 - 5\tau - 12\phi_0^2})$. In this case the Lamé constants $\lambda$ and $\mu$ and the 2D Young modulus $K_0$ can be expressed as $\lambda = 30|A_k|^2k_0^2$, $\mu = 6|A_k|^2k_0^2$, and $K_0 = \frac{4\mu(\mu+\lambda)}{2\mu+\lambda}$. Here we select the temperature and free-energy parameters in order to allow the defect-induced buckling transition. We consider only membranes with fixed genus where the free-energy parameters were fixed at $\phi_0 = 0.4$, $\tau = 0$, $\sigma = 1.1$, $k_B = 0.1$, and $C_0 = 0$. Figure 3 shows the time evolution of a membrane suffering a symmetry-breaking phase transition when it is quenched below the critical temperature $T_c$. As we show below, the topography of the membrane is strongly coupled with the motion of the defects and vice versa.

It has been observed in different systems that the strain field induced by a disclination affects its core radius [53]. In response to the defect core energy, the domains at lattice defect sites adjust their sizes relative to domains with sixfold coordination (positive disclinations contract and negative disclinations expand). In planar systems, this local deformation has been observed in films of block copolymers and magnetic garnets [58,59]. While this effect appears to have no effect on the dynamics of coarsening in planar systems [55], here we found that the positive disclinations can easily relax the strain field stored in the core by buckling out of the plane (see Fig. 4). Thus, the energetic asymmetry between disclinations of different sign does not only modify the effective Kosterlitz-

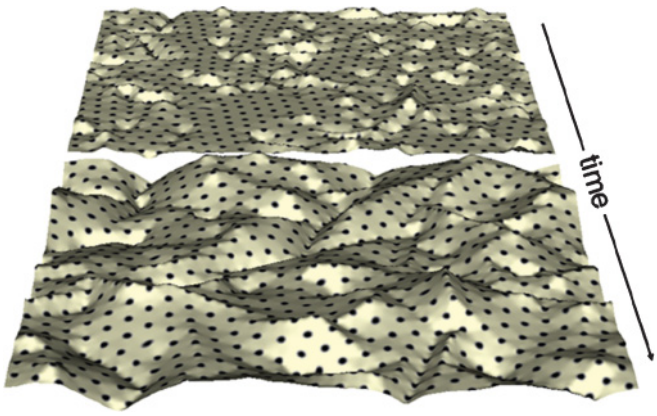


FIG. 3. (Color online) Coarsening kinetics of a crystalline membrane suffering a symmetry-breaking phase transition. A crystalline membrane can buckle out of the plane driven by the relaxation of the strain field introduced by topological defects. During the temporal evolution toward equilibrium the annihilation and diffusion of topological defects is dictated by the strong coupling between the membrane shape and the geometrically screened strain field associated with the defects.

Thouless transition temperature of the membrane [24], but also dictates the early dynamics of buckling. Since the diffusion of defects is affected by the geometric potential, the long time relaxation of the system becomes tightly linked to the early stage of buckling.

At the early stage of buckling, the compressional strain field of the lattice in the neighborhood of a positive disclination can induce the buckling of the membrane in either side of the flat reference configuration ($h = 0$). While the energy corresponding to isolated buckled disclinations is independent of the direction of buckling ($h < 0$ or $h > 0$), as two disclinations become closer, the energy depends on the degree of overlap between the membrane deformation induced by each disclination. It has been noted by Carraro and Nelson (CN) that buckling in opposite directions is favored for defects that are further apart than two lattice constants [56]. This CN or "antiferromagnetic" interaction between defects is favored by the bending energy of the membrane. At the early stage of buckling, the interspace between topological defects is nearly flat because the deformation is concentrated at the core of the disclinations and there is no substantial overlap between the deformation induced by the different defects [Fig. 4(a)]. Thus, the buckling introduced by the positive disclinations in the upward ($h > 0$) or downward ($h < 0$) directions is predominantly random. As time proceeds, there is an increase in the membrane deformation and the bending energy controls the direction of buckling [Fig. 4(b)]. In order to identify the existence of CN interactions during the relaxation of the crystalline membrane, we define a disclination-disclination pair correlation function $C(s)$ that takes into account the direction of buckling:

$$C(s) = \langle \rho(r,t)\rho(r-s,t)\Upsilon(r)\Upsilon(r-s)\rangle, \qquad (5)$$

where $\rho(r,t)$ is the density of topological defects, $\langle\cdots\rangle$ denotes an ensemble average with all the disclination pairs, $s$ is the geodesic distance between defects, and $\Upsilon(\mathbf{x}) = h(\mathbf{x})/|h(\mathbf{x})|$ takes into account the sign of the CN interactions [i.e., the

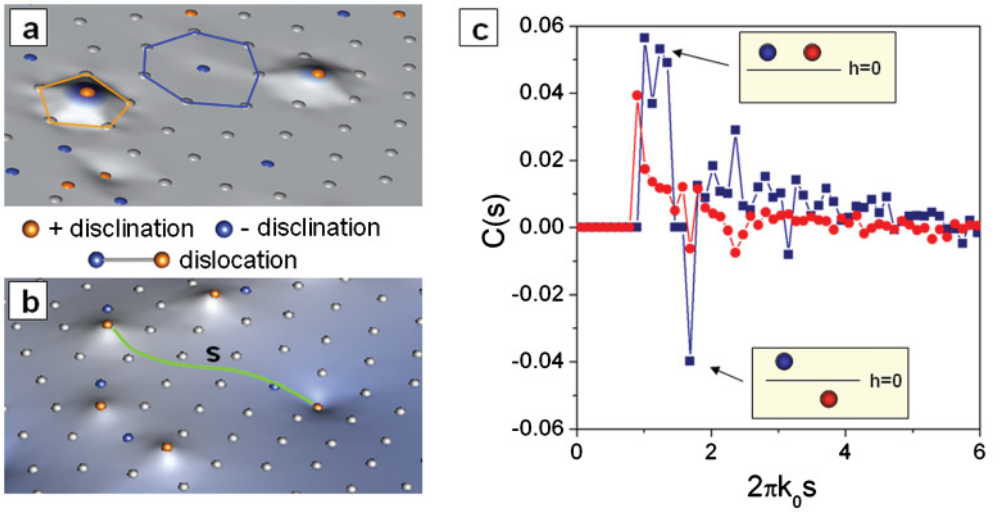


FIG. 4. (Color online) (a) The positive disclinations involved into the dislocations relax the stress field of the lattice by buckling out of the plane. (b) Favored by the bending energy, the buckling of the membrane in opposite directions produces metastable configurations of defects. Here the green (gray) line represents the geodesic distance $s$ between two positive disclinations. (c) $C(s)$ as a function of $s$ at the onset of the buckling transition (circles) and at long times (squares).

sign of $\Upsilon(r)\Upsilon(r-s)$ determines if the buckling introduced by a pair of defects is in either the same side or opposite sides of the flat reference configuration] [60].

Figure 4(c) also shows the pair correlation function $C(s)$ at two different time scales. At the onset of the buckling transition $C(s)$ shows a maximum at the position corresponding to the average distance between the positive and negative disclinations forming a dislocation. Driven by the coupling between the defects and geometry of the membrane, at large time scales there is a splitting of the main peak of $C(s)$, associated to the unbinding of the positive and negative disclinations. In addition, it is also possible to observe local minima at a distance slightly smaller than two lattice spacings, indicating the presence of CN interactions between near defects. Both mechanisms slow down the dynamics. The unbinding of the dislocations stabilizes the position of the positive disclinations by increasing the membrane deformation. Thus, the binding geometrical potential generated by the membrane deformation slows down the dynamics of particles and defects in the neighborhood of the dynamically stabilized positive disclinations. On the other hand, the increase of the CN interactions produces dynamically metastable configurations of defects, like those shown in Fig. 4(b), that also slow down the dynamics.

In flat crystals the pathways toward equilibrium involve the diffusion of dislocations located along grain boundaries. In these systems it has been found that the rate of defect annihilation is not controlled by the glide motion of dislocations but for the slow diffusion of triple points (bounded regions where three misoriented grains meet) [38,55]. As a consequence of the pinning of triple points, in flat systems the temporal evolution of the correlation length depends logarithmically on time (Lifshitz-Safran mechanism) [52,61,62]. On the other hand, in frozen curved topographies it has been determined that the local curvature acts as a geometric potential that strongly affects the motion of defects [19,63].

In order to analyze the dynamics of the system, here we track the motion of the particles and defects. Once the position of the particles (defects) was identified, the trajectories were determined through $\rho(\mathbf{r}) = \sum_{i=1}^{N} \delta[\mathbf{r} - \mathbf{r}_i(t)]$, where $\mathbf{r}_i(t)$ is the position of the particle (defect) $i$ at time $t$. Figure 5 compares the time evolution of the average density of topological defects $\rho_{\text{def}}$ in flat and buckled systems. As expected, at short time scales, where the polycrystalline structure is defined, $\rho_{\text{def}}$ is approximately the same in both systems. However, at large time scales ($t > 100t_0$) $\rho_{\text{def}}$ in the buckled membrane is systematically higher than in flat crystals, indicating a slower mechanism of defect annihilation [64].

The role of the buckling onto the relaxational dynamics can also be analyzed by tracking the diffusion of the individual particles in the system. The dynamics of particle diffusion in 2D crystals with hexagonal symmetry has been studied in colloidal

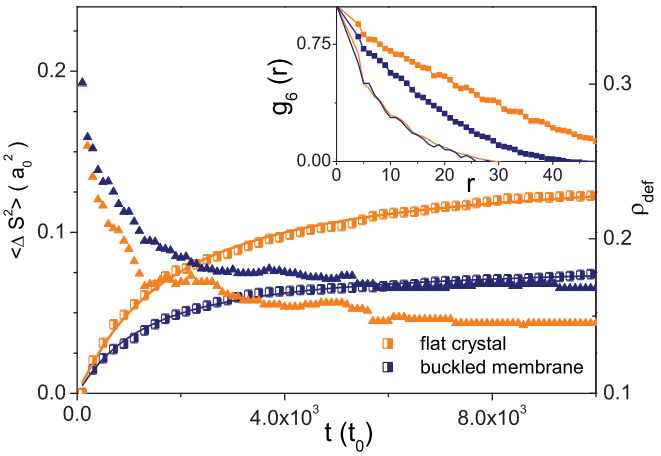


FIG. 5. (Color online) Diffusion coefficient (squares) and dislocation density (triangles) as a function of time in flat and buckled membranes. In the buckled membrane, both disclination unbinding and CN interactions slow down the dynamics of coarsening below the Lifshitz-Safran regime. Inset: $g_6(r)$ over the reference plane $h = 0$ as function of $r$ at early (lines) and long times (symbols).

systems on different geometries [18,63]. Taking into account the free diffusion of particles at short times and approximating the restoring potential between near neighbor particles by a circularly symmetric harmonic interaction $W(r) = \frac{1}{2}k_s r^2$ centered about each particle equilibrium position ($k_s$ being a effective spring stiffness), the time dependence of the average mean square displacement of the particles $\langle \Delta s^2 \rangle$ can be described by the following two-parameter model [18,65]:

$$\langle \Delta s^2 \rangle = \frac{1}{2} \frac{k_s \beta + \frac{1}{4Dt}}{\left[\frac{k_s \beta}{2} + \frac{1}{4Dt}\right]^2}. \quad (6)$$

Here $D$ is the diffusion constant and $\beta = 1/k_B T$ is the thermal energy [66]. Figure 5 also shows the time evolution of $\langle \Delta s^2 \rangle$ in flat and buckled membranes. A standard regression fit through the data with the model for $\langle \Delta s^2 \rangle$ yields $D = 3.010^{-5} a_0^2$ and $k_s = k_s^f = 14\beta/a_0^2$ for the flat crystal and $D = 2.510^{-5} a_0^2$ and $k_s = k_s^m = 24\beta/a_0^2$ for the buckled membrane. Thus, the strength of the harmonics traps involved in the long time relaxation of the buckled membrane are very large as compared with the flat counterpart ($k_s^m/k_s^f \sim 1.7$) while the diffusion coefficient becomes about 20% smaller, in agreement with the results for the dynamics of defects. Note that here the nature of the interactions responsible for the slowing down is completely different.

The inset of Fig. 5 shows the azimuthally averaged correlation function $g_6(r) = \langle \exp[6i(\theta(\mathbf{r} + \mathbf{r}') - \theta(\mathbf{r}'))] \rangle$, defined in terms of the local bond orientation $\theta(\mathbf{r})$ [55]. Consistently with the data for $\langle \Delta s^2 \rangle$ and $\rho_{\text{def}}$, we clearly observe that the orientational dynamics is slower in the membrane (at long times the orientational correlation length is about 40% smaller than in the flat crystal).

Thus, while in flat systems the dynamics becomes slow as a consequence of the pinning of triple points, in crystalline membranes the pinning of positive disclinations and Carraro-Nelson interactions control the dynamics.

## IV. CONCLUSIONS

In summary, the early dynamics of buckling is led by the positive disclinations. The coupling between the the topography of the membrane and the defects induces the pinning of positive disclinations and the formation of metastable structures of defects, stabilized by CN interactions. Consequently, the relaxational dynamics of the system becomes even slower than the Lifshitz-Safran regime observed in flat crystals. The Brazovskii-Helfrich-Canham approach described here provides a general framework for studying the dynamics of topological defects in crystalline membranes, and can be straightforwardly extended to crystalline phases with different symmetries.

## ACKNOWLEDGMENTS

We acknowledge helpful discussions with L. Gómez, T. Lubensky, and D. Nelson. This work was supported by Universidad Nacional del Sur, the National Research Council of Argentina (CONICET), and the National Science Foundation (CONICET-NSF program) through Princeton University and Instituto de Física del Sur.

[1] M. Seul and D. Andelman, Science **267**, 476 (1997).
[2] C. Harrison, D. H. Adamson, Z. Cheng, J. M. Sebastian, S. Sethuraman, D. A. Huse, R. A. Register, and P. M. Chaikin, Science **290**, 1558 (2000).
[3] A. V. Ruzzete and L. Leibler, Nat. Mater. **4**, 19 (2005).
[4] A. K. Geim and K. S. Novoselov, Nat. Mater. **6**, 183 (2007).
[5] L. Tsarkova, A. Knoll, and R. Magerle, Nano Lett. **6**, 1574 (2006).
[6] M. Ma, K. Titievsky, E. L. Thomas, and G. C. Rutledge, Nano Lett. **9**, 1678 (2009).
[7] Y. S. Jung and C. A. Ross, Nano Lett. **7**, 2046 (2007).
[8] C. Harrison, Z. Cheng, S. Sethuraman, D. A. Huse, P. M. Chaikin, D. A. Vega, J. M. Sebastian, R. A. Register, and D. H. Adamson, Phys. Rev. E **66**, 011706 (2002).
[9] R. A. Segalman, Mater. Sci. Eng. R **48**, 191 (2005).
[10] D. R. Nelson, Nano Lett. **10**, 1125 (2002).
[11] G. A. DeVries, M. Brunnbauer, Y. Hu, A. M. Jackson, B. Long, B. T. Neltner, O. Uzun, B. H. Wunsch, and F. Stellacci, Science **315**, 358 (2007).
[12] E. V. Yazyev and E. G. Louie, Nat. Mater. **9**, 806 (2010).
[13] A. R. Bausch *et al.*, Science **299**, 1716 (2003).
[14] R. D. Kamien, Science **299**, 1671 (2003).
[15] A. Hexemer, V. Vitelli, E. J. Kramer, and G. H. Fredrickson, Phys. Rev. E **76**, 051604 (2007).
[16] T. L. Chantawansri, A. W. Bosse, A. Hexemer, H. D. Ceniceros, C. J. Garcia-Cervera, E. J. Kramer, and G. H. Fredrickson, Phys. Rev. E **75**, 031802 (2007).
[17] L. Giomi and M. Bowick, Phys. Rev. B **76**, 054106 (2007).
[18] P. Lipowsky *et al.*, Nature Mat. **4**, 407 (2005).
[19] L. R. Gómez and D. A. Vega, Phys. Rev. E **79**, 031701 (2009).
[20] D. R. Nelson, Phys. Rev. B **28**, 5515 (1983).
[21] S. Sachdev and D. R. Nelson, J. Phys. C **17**, 5473 (1984).
[22] H. S. Seung and D. R. Nelson, Phys. Rev. A **38**, 1005 (1988).
[23] J. M. Park and T. C. Lubensky, Phys. Rev. E **53**, 2648 (1996).
[24] J. M. Park and T. C. Lubensky, J. Phys. I (France) **6**, 493 (1996).
[25] J. L. Harden, F. C. MacKintosh, and P. D. Olmsted, Phys. Rev. E **72**, 011903 (2005).
[26] F. Cavallo and M. G. Lagally, Soft Matter **6**, 439 (2010).
[27] J. S. Lowengrub, A. Raätz, and A. Voigt, Phys. Rev. E **79**, 031926 (2009).
[28] P. Sunil Kumar, G. Gompper, and R. Lipowsky, Phys. Rev. Lett. **86**, 3911 (2001).
[29] H. Popova and A. Milchev, Phys. Rev. E **77**, 041906 (2008).
[30] D. Moldovan and L. Golubovic, Phys. Rev. E **60**, 4377 (1999).
[31] F. J. Solis, C. M. Funkhouser, and K. Thornton, Europhys. Lett. **82**, 38001 (2008).
[32] W. T. Gozdz and G. Gompper, Europhys. Lett. **55**, 587 (2001).
[33] C. M. Funkhouser, F. J. Solis, and K. Thornton, Phys. Rev. E **76**, 011912 (2007).

[34] W. Helfrich, Z. Naturforsch. C **28**, 693 (1973).
[35] P. B. Canham, J. Theor. Biol. **26**, 61 (1970).
[36] Ou-Yang, Zhong-Can and W. Helfrich, Phys. Rev. A **39**, 5280 (1989).
[37] I. S. Sokolnokoff, *Theory and Applications to Geometry and Mechanics of Continua* (Wiley, New York, 1964).
[38] D. A. Vega, C. K. Harrison, D. E. Angelescu, M. L. Trawick, D. A. Huse, P. M. Chaikin, and R. A. Register, Phys. Rev. E **71**, 061803 (2005).
[39] K. R. Elder, M. Katakowski, M. Haataja, and M. Grant, Phys. Rev. Lett. **88**, 245701 (2002).
[40] A. D. Pezzutti, D. A. Vega, and M. A. Villar, Phil. Trans. R. Soc. A **369**, 335 (2011).
[41] K.-A. Wu and A. Karma, Phys. Rev. B **76**, 184107 (2007).
[42] J. Mellenthin, A. Karma, and M. Plapp, Phys. Rev. B **78**, 184110 (2008).
[43] K. Yamada and S. Komura, J. Phys. Condens. Matter **20**, 1 (2008).
[44] D. A. Vega and L. R. Gómez, Phys. Rev. E **79**, 051607 (2009).
[45] A. D. Pezzutti, L. R. Gómez, M. A. Villar, and D. A. Vega, Europhys. Lett. **87**, 66003 (2009).
[46] I. W. Hamley, *The Physics of Block Copolymers* (Oxford University Press, New York, 1998).
[47] A. Andelman, F. Brochard, and J. Joanny, J. Chem. Phys. **86**, 3673 (1987).
[48] J. Swift, Phys. Rev. A **14**, 2274 (1976).
[49] S. A. Brazovskii, Sov. Phys. JETP **41**, 85 (1975).
[50] D. R. Nelson, *Defects and Geometry in Condensed Matter Physics* (Cambridge University Press, Cambridge, United Kingdom, 2002).
[51] R. D. Kamien, Rev. Mod. Phys. **74**, 953 (2002).
[52] L. R. Gómez, E. M. Vallés, and D. A. Vega, Phys. Rev. Lett. **97**, 188302 (2006).
[53] P. M. Chaikin and T. C. Lubensky, *Principles of Condensed Matter Physics* (Cambridge University Press, Cambridge, United Kingdom, 1995).
[54] A. Travesset, Phys. Rev. B **68**, 115421 (2003).
[55] C. Harrison *et al*., Europhys. Lett. **67**, 800 (2004).
[56] C. Carraro and D. R. Nelson, Phys. Rev. E **48**, 3082 (1993).
[57] K. Kawasaki and T. Otha, Physica A **139**, 223 (1986).
[58] M. R. Hammond, S. W. Sides, G. H. Fredrickson and E. J. Kramer, Macromol. **36**, 8712 (2003).
[59] M. Seul and C. A. Murray, Science **262**, 558 (1993).
[60] Here the maximum membrane deformation $h = h_{\max}$ remains relatively small ($h_{\max} < 2a_0$). Then, $\Upsilon(\mathbf{x})$ provides a good approximation to determine the CN interactions.
[61] L. M. Lifshitz, Sov. Phys. JETP **15**, 939 (1962).
[62] S. A. Safran, Phys. Rev. Lett. **46**, 1581 (1981).
[63] V. Vitelli, J. V. Lucks, and D. R. Nelson, PNAS **33**, 12323 (2006).
[64] See Supplemental Material at http://link.aps.org/supplemental/10.1103/PhysRevE.84.011123 for a movie.
[65] J. A. Weiss, A. E. Larsen, and D. G. Grier, J. Chem. Phys. **109**, 8659 (1998).
[66] Similarly to previous works [18,65], here we also observe that the structural contribution to $\langle \Delta s^2 \rangle$ is very small.